electronics

MDPI

Article

Optimal GPS Acquisition Algorithm in Severe Ionospheric Scintillation Scene

Mengying Lin [1], Yimei Luo [1], Xuefen Zhu [1,*], Gangyi Tu [2] and Zhengpeng Lu [1]

[1] Key Laboratory of Micro-Inertial Instrument and Advanced Navigation Technology of Ministry of Education, School of Instrument Science and Engineering, Southeast University, Nanjing 210096, China
[2] School of Electronic and Information Engineering, Nanjing University of Information Science and Technology, Nanjing 210044, China
* Correspondence: zhuxuefen@seu.edu.cn; Tel.: +86-13645161372

Abstract: The Global Positioning System (GPS) plays an important role in navigation and positioning services. When GPS signals propagate through a complex space environment, they are susceptible to interference of ionospheric scintillation. As one of the biggest interference sources on GPS navigation and positioning, ionospheric scintillation will lead to signal intensity decline and carrier phase fluctuation, making signal acquisition of the GPS receiver challenging. Thus, an acquisition algorithm based on differential coherent integration combining accumulation correlation and bit sign transition estimation is proposed. The coherent accumulation is applied to reduce computational loads and contribution by the Gaussian white noise in the signal. Moreover, the differential coherence integration is utilized to eliminate data blocks with bit transition, prolonging the coherence integration time and improving the data utilization rate. Experimental results show that under severe ionospheric scintillation condition, weak GPS signals can be acquired successfully after improving the acquisition algorithm, with the acquisition probability reaching 50% when the signal-to-interference ratio (SIR) drops to −34 dB. Comparing to the differential coherence integration, the complexity of the calculation reduces to only 21.75% effectively after the improvement. The execution time is less than half of the differential coherence integral.

Keywords: GPS acquisition; coherent accumulation; bit sign transition; differential coherent integration; ionospheric scintillation

Citation: Lin, M.; Luo, Y.; Zhu, X.; Tu, G.; Lu, Z. Optimal GPS Acquisition Algorithm in Severe Ionospheric Scintillation Scene. *Electronics* **2023**, *12*, 1343. https://doi.org/10.3390/electronics12061343

Academic Editor: Arturo de la Escalera Hueso

Received: 13 February 2023
Revised: 5 March 2023
Accepted: 10 March 2023
Published: 12 March 2023

1. Introduction

GPS plays a critical role in economic, infrastructure, social development, national defense, and security [1], providing continuous positioning and timing services for various applications, including civilian and military use. To ensure successful navigation and positioning, the acquisition and tracking modules are essential for software receivers, requiring a rough estimation of carrier frequency and code phase [2]. However, GPS signals are susceptible to distortion when passing through complex environments, such as adverse weather, dense building occlusion in cities, and multipath effects [3]. Such phenomena will disrupt the code and carrier parameters of a GPS receiver, and even result in the loss of GPS signal acquisition and tracking, making it impossible to obtain positioning information. Ionospheric scintillation, one of the main sources of GPS signal interference, frequently occurs in low latitude regions and can lead to decreased carrier-to-noise ratio (C/N_0) of the signal, making it difficult to capture by receivers, resulting in cycle slips, phase errors, and increased carrier Doppler shifts [4]. This ultimately leads to a degradation in position and navigation solution accuracy [5], as illustrated in Figure 1. In light of these extreme space weather interferences, it is necessary to study weak signal receiver acquisition algorithms that are low in calculation and high in speed. Moreover, quick and accurate signal reacquisition is critical to ensure the tracking robustness of the receiver once it loses lock due to severe ionospheric scintillation interference.

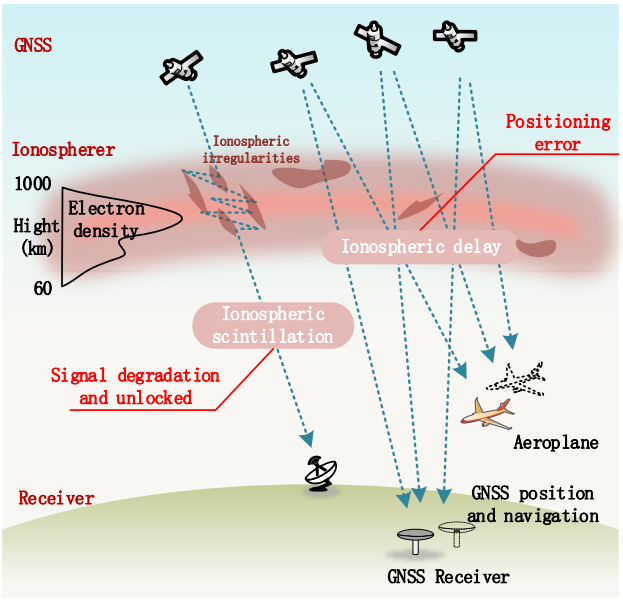

Figure 1. Ionospheric effects on GNSS signals.

In early GPS receivers, a serial acquisition algorithm was commonly used, which had high computational complexity and long acquisition times. To address these issues, parallel frequency space acquisition and parallel code phase acquisition algorithms were proposed, significantly improving acquisition speed, but these methods are not suitable for weak signal environments. Coherent integration methods, including coherent, non-coherent, and differential coherent integration, are generally used to improve the signal-to-interference ratio (SIR) and address signal acquisition challenges in weak signal environments [6]. Coherence integration is the most effective method to improve SIR gain, but is sensitive to navigation bit sign transition. Lin et al. pointed out that non-coherent integration is effective only with a small number of integrals [7]. Hussain et al. proposed an adaptive data length method for acquisition by adjusting the times of non-coherent integration according to levels of noise and signal power, but it is also restricted to bit transition [8]. Elders-Boll et al. proposed differential coherence integration to reduce square loss while retaining incoherent integration's insensitivity to the data bit jump [9]. However, this method decreases the number of useful satellite signals, limiting SIR gain. Huang et al. proposed a method based on block zero compensation to eliminate data with a bit jump by splitting and zero filling, and then performing incoherent integration to capture the weak signal [10]. However, this method requires large computational resources and has a slow operation speed. Combining coherent and incoherent integration can effectively improve signal-to-noise ratio (SNR) gain by dividing data into blocks, performing coherent integration first, and then incoherent accumulation [11]. Nevertheless, this method has a maximum data length of 20 ms and experiences some loss in incoherent integration. Jeon et al. discussed the bit transition problem of GPS L2-CM and L5 signals, having a data bit duration of the same as the code period length, which is totally different from the GPS L1 signal [12]. In addition, comparative experiments are conducted on three acquisition strategies of coherent, non-coherent, and differential coherence algorithms. It is found that the coherent channel combination has the best performance, but the relative sign between the estimated data and the pilot frequency is required [13,14].

To summarize, there are several shortcomings on dealing with acquisition problems during a severe ionospheric scintillation scene, as listed in the following:

(1) Serial acquisition algorithm is slow and computationally complex;
(2) Parallel frequency space and parallel code phase acquisition algorithms are ineffective in a weak signal;

(3) Coherent integration is sensitive to navigation bit sign transition and non-coherent integration is only useful with fewer integrals;
(4) Block zero compensation has limitations in data length and loss of incoherent integration.

As a solution to the drawbacks mentioned above and aiming at the acquisition of weak satellite signals caused by ionospheric scintillation, an acquisition algorithm based on differential coherent integration combined with coherent accumulation and bit sign transition estimation is proposed in the framework of a parallel code phase acquisition algorithm. Based on the differential coherent integration, the coherent accumulation is combined to reduce the noise in the signal and realize fast acquisition. The bit transition estimation is combined to exclude data with bit transition, prolong the coherence integration time, and realize weak signal acquisition with severe ionospheric scintillation.

The remaining part of the article is organized as follows: Section 2 briefly introduces the principles of the signal acquisition algorithm. Section 3 introduces the methodology, especially the accumulation correlation, bit sign transition estimation, and implementation process. Section 4 introduces the results of experiments and analyzes the effects of the algorithm. Section 5 concludes the effectiveness of the proposed methods.

2. Basic Principles of Signal Acquisition

2.1. Parallel Code Phase Acquisition Algorithm

In this paper, a parallel code phase acquisition algorithm is selected as the basis because the execution time of single satellite acquisition is far less than serial acquisition and parallel frequency space acquisition, which will greatly decrease the computation complexity and increase acquisition speed. The following principle of the parallel code phase acquisition algorithm, which is obtained in [15], will be briefly introduced.

In order to make a circular cross correlation between the input signal and the local signal without the shifted code phase, a method of performing circular correlation through Fourier transforms will be described.

Suppose there are finite sequences $x(n)$ and $y(n)$, both with length N: the circular cross-correlation sequence between $x(n)$ and $y(n)$ is computed as:

$$z(n) = \frac{1}{N}\sum_{m=0}^{N-1} x(m)y(m-n). \tag{1}$$

In the following, the scaling factor $\frac{1}{N}$ will be omitted. After the N-points Fourier transform, $z(n)$ can be expressed as:

$$\begin{aligned} z(n) &= \sum_{n=0}^{N-1}\sum_{m=0}^{N-1} x(m)y(m-n)e^{\frac{-j2\pi kn}{N}} \\ &= \sum_{m=0}^{N-1} x(m)e^{\frac{-j2\pi kn}{N}} \sum_{n=0}^{N-1} y(m-n)e^{\frac{j2\pi k(n-m)}{N}} \\ &= X(k)Y^*(k) \end{aligned} \tag{2}$$

where $Y^*(k)$ is the complex conjugate of $Y(k)$.

A schematic diagram of the parallel code phase search algorithm is shown in Figure 2. The input signal is multiplied by the locally generated carrier signal to obtain in-phase I signal and quadrature-phase Q signal, which are regarded as the real and imaginary parts of the complex signal $x(n)$, respectively; $x(n)$ can be expressed as:

$$x(n) = I(n) + jQ(n). \tag{3}$$

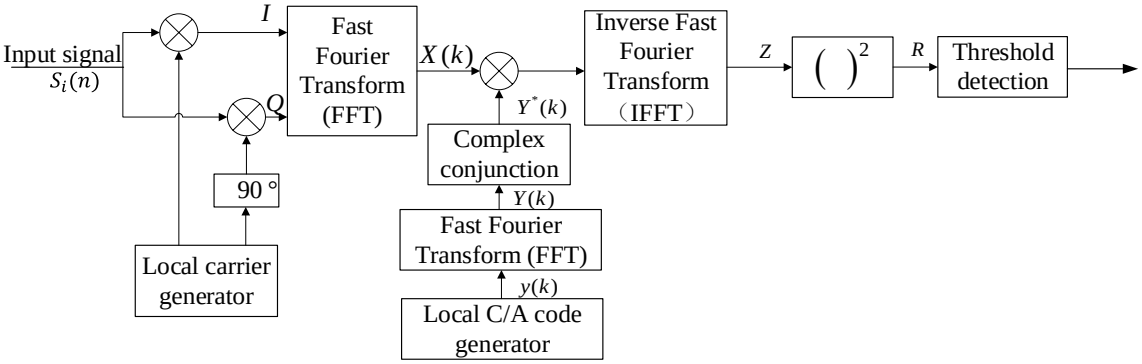

Figure 2. The schematic diagram of the parallel code phase search algorithm.

The generated C/A code is transformed into the frequency domain and the result is complex conjugated.

After the fast Fourier transform (FFT) of the $x(n)$ being multiplied with the FFT of the C/A code, the result of the multiplication is transformed into the time domain by the inverse fast Fourier transform (IFFT). The absolute value of the IFFT output Z represents the correlation between the complex signal and the C/A code. If there is a peak in the correlation, the index of this peak marks the C/A code phase of the input signal. In this paper, the added result of correlation elements after squaring is taken as the final decision result R. The ratio of the peak R to the second largest peak v is compared to the threshold, so as to determine whether the acquisition is successful.

2.2. Differential Coherent Integration

The differential coherence integration computes the correlation values of two adjacent moments by conjugate multiplication and then accumulates the outcomes [16,17]. The schematic diagram is shown in Figure 3.

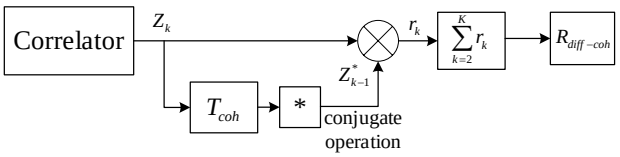

Figure 3. The schematic diagram of differential coherence integration.

The formula for the decision result $R_{diff-coh}$ is as follows:

$$\begin{aligned} R_{diff-coh} &= \left| \sum_{k=2}^{N} Z_k Z_{k-1}^* \right|^2 \\ &= \left| \sum_{k=2}^{N} (I_k + jQ_k)(I_{k-1} + jQ_{k-1})^* \right|^2 \\ &= \left| \sum_{k=2}^{N} [(I_k I_{k-1} + Q_k Q_{k-1}) + j(Q_k I_{k-1} + I_k Q_k)] \right|^2 \end{aligned} \tag{4}$$

where the Z_k is the kth coherent integral result, N is the number of incoherent accumulations in differential coherence, and Z_{k-1}^* is the complex conjugate of Z_{k-1}.

In general, it is assumed that the input signal and the local reference signal are in perfect synchronization with no code phase shift and no Doppler frequency residual. The signal mainly exists in the I branch, and the Q branch is the noise after the coherent

integration. In the sequence data, signal amplitude is unchanged, and the mean value of noise is 0. In this case, $Q_k I_{k-1} + I_k Q_k \approx 0$, Equation (4) can be replaced as:

$$R_{diff-coh} = \left| \sum_{k=2}^{N} (I_k I_{k-1} + Q_k Q_{k-1}) \right|^2. \quad (5)$$

Currently, most of the processing and analysis of the differential and integral algorithms used is based on Equation (5), because of the simplicity of their explicit expressions.

However, in the real weak signal environment, because of inevitable Doppler residual, the signal exists not only in the authentic part, but also in the imaginary part of the output. Therefore, if only the authentic part of the signal is taken for detection, such as the simple expressions of Equation (5), the signal energy will be lost, leading to poor acquisition performance. As a solution to this problem, this paper will use the full expression of the equation, which is Equation (4).

3. Methodology

3.1. Coherent Accumulation Principle

Coherent integration is the correlation between satellite signals and local replication signals of equal length. With the extension of integration time, the points of FFT/IFFT operations for satellite signals and local replication signals will increase exponentially, which will lead to a sharp increase in the amount of computation and a decrease in the acquisition speed. Meanwhile, non-coherent integration squares correlated values so that the noise is squared at the same time, introducing considerable new noise into correlation results, which is always called squaring loss. With the increase in accumulation times, the squaring loss increases, which significantly affects the performance of integration.

Therefore, this paper adopts the method of coherent accumulation. The signal to be processed is superposed, and then FFT is used for correlation calculation [18]. Its principle is as follows: assume that $x_l(t_n)$ is the received signal to calculate correlation, with a length of 1 ms; $y(t_n)$ is the C/A code signal replicated locally. As mentioned above, the relevant operation can be expressed as:

$$Z(k) = X_l(k) Y^*(k) \quad (6)$$

where $X_l(k)$ represents FFT of $x_l(t_n)$, $Y^*(k)$ is obtained by the complex conjugate of $y(t_n)$ through FFT.

Assuming that the correlation accumulation length of signals is L ms, the correlation accumulation times are L:

$$\begin{aligned} Z_\Delta(k) &= \sum_{l=1}^{L} X_l(k) Y^*(k) \\ &= Y^*(k) \sum_{l=1}^{L} FFT[x_l(t_n)] \\ &= Y^*(k) \mathrm{FFT} \left[\sum_{l=1}^{L} x_l(t_n) \right]. \end{aligned} \quad (7)$$

Therefore, the C/A code periodic signals that need to be accumulated are first superimposed, and then calculated for correlation coefficients based on FFT. Only one correlation operation and a small amount of accumulation operation are required to obtain the results of multiple correlation operations.

For example, if the sampling frequency is 6 Mhz, that is, there are 6000 points per C/A code cycle, the number of points required to perform FFT is $6000L$ points for traditional coherence integration of L ms data. As for L ms data accumulation, the accumulation method is shown in Figure 4. In this way, only 6000 points need FFT operation. Coherent accumulation not only reduces the computation complexity and improves the acquisition speed, but also multiplies the amplitude of the useful signal while ensuring that the mean of the white Gaussian noise is still 0.

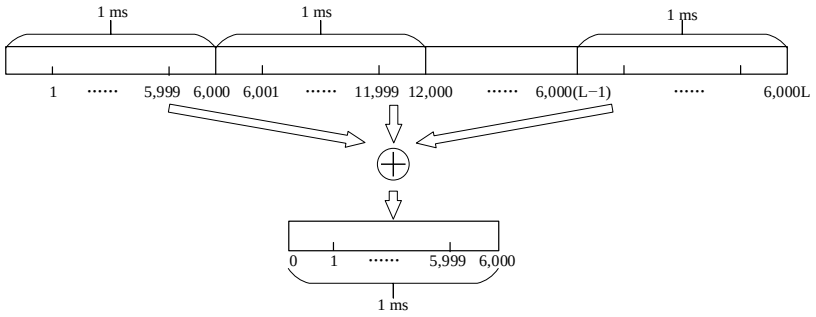

Figure 4. Schematic diagram of coherent accumulation.

3.2. Bit Shift Estimation Principle

Although differential coherence integration is less sensitive to bit sign transition than coherence integration, differential coherence integration cannot completely eliminate the effect caused by bit shifts. Assuming that 20 ms data with bit sign transition exists in each processing, and every 4 ms data are treated as a data block, a total of five data blocks are superimposed and correlated, respectively. The navigation data bits corresponding to each data block are $D_a = +1$, $D_b = +1$, $D_c = -1$, $D_d = -1$, and $D_e = -1$. Data blocks $D_a D_b^* = +1$, $D_b D_c^* = -1$, $D_c D_d^* = +1$, and $D_d D_e^* = +1$ are obtained by conjugate multiplication of adjacent. The result of differential coherent integration is $D_a D_b^* + D_b D_c^* + D_c D_d^* + D_d D_e^* = 1$. As can be seen, in this case, the acquisition results are severely attenuated. Therefore, bit sign transition estimation is utilized in this paper, with its principle shown in Figure 5. In order to overcome the influence of bit sign transition, record the minimum value after conjugate multiplication of the correlation values of adjacent data blocks of 4 ms, and eliminate this minimum value caused by bit sign transition [19].

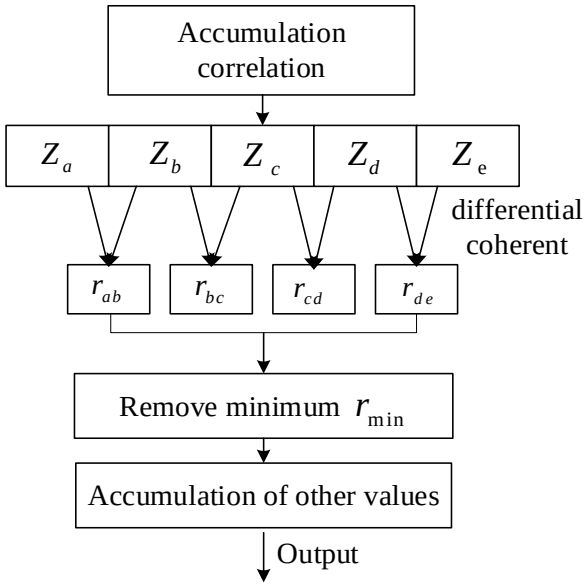

Figure 5. Schematic diagram of bit sign transition estimation.

3.3. Algorithm Implementation Process

The schematic diagram of the acquisition algorithm based on differential coherent integration combining coherent accumulation and bit sign transition estimation proposed in this paper is shown in Figure 6.

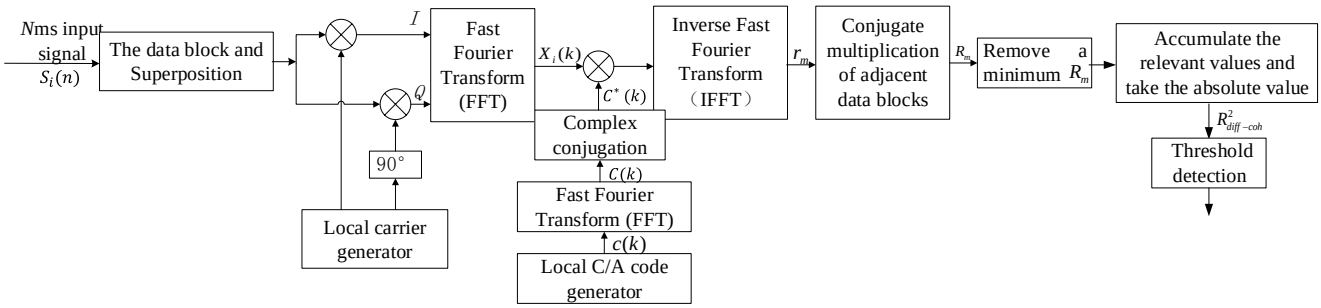

Figure 6. Schematic diagram of the acquisition algorithm based on differential coherent integration combining coherent accumulation and bit sign transition estimation.

The specific implementation steps are as follows:

(a) Divide the data of continuous N ms into M data blocks. The length of each data block is L, $N = M \times L$;

(b) Accumulate each data block in step (a), separately;

(c) Generate in-phase and ortho-phase carriers by the carrier generator. They are multiplied by the accumulation result of step (b) to obtain I and Q signals, which are the authentic and imaginary parts of the complex signal $X_i(k)$, $i = 1, 2, 3, \cdots, M$, respectively;

(d) Transform the local code generated by the local C/A code generator into the frequency domain by FFT and obtain its complex conjugate $C^*(k)$;

(e) Multiply the corresponding elements of complex signal $X_i(k)$ and $C^*(k)$, getting IFFT result $r_i(k)$;

(f) Conjugate the correlation values of adjacent blocks, $R_m^2 = r_{m-1}^* r_m, m = 2, 3, \cdots, M$;

(g) Compare all R_m^2, and select the minimum $R_m^2 = R_n^2$ and then remove. It is considered that there is bit sign transition in this section of data;

(h) Obtain the final decision value is $R_{diff-coh}^2$ based on the absolute value of the remaining R_m^2:

$$R_{diff-coh}^2 = \sum_2^m R_m^2, \ m \neq n; \tag{8}$$

(i) Determine whether the ratio of the peak value $R_{diff-coh}^2$ to the second largest peak value is greater than the threshold. If it is greater than the threshold, the acquisition is successful. Otherwise, the local carrier and code phase are adjusted for the next acquisition.

4. Results

4.1. Experimental Settings

In this section, the acquisition effect, acquisition probability, and acquisition speed of the four acquisition algorithms are compared and analyzed. For convenience of expression, the improved differential coherent integration acquisition algorithm below refers to the proposed weak signal acquisition algorithm based on differential coherent integration combining coherent accumulation and bit sign transition estimation proposed in this paper. It is assumed that the length of data acquired by the four methods is 20 ms. The following Table 1 lists the specific settings of the four acquisition algorithms:

In order to compare and analyze the four acquisition algorithms, this paper simulates intermediate frequency satellite signals with different SIR in the Matlab environment. The intermediate frequency of simulation data was set to 0, the sampling frequency was set to 3 MHz, the signal was superimposed with Gaussian white noise, and the SIR was set from -40 to -22 dB with an interval of 1 dB.

Table 1. Experimental acquisition algorithm-specific settings.

Acquisition Algorithm	Parameter Settings
Coherent integration	Coherent integration time: 20 ms
Coherent and non-coherent integration	Coherent integration time: 2 ms Number of incoherent accumulations: 10 times
Differential coherent integration	Coherent integration time: 1 ms Number of differential coherent integration: 19 times
Improved differential coherent integration	Coherent accumulation time: 2 ms Number of differential coherent integration: 9 times

4.2. Evaluation of Acquisition Effects

Firstly, the effects of different acquisition algorithms under different SIR are compared. Generally, satellite signals with SIR less than −22 dB are called weak signals [20]. In this paper, the ratio of the largest peak value to the second largest peak value is used to determine whether the acquisition is successful. The acquisition threshold is set to 2.3 and the search step is set to 500 Hz. In order to compare, the simulated signal of the satellite number 10 (PRN10) was used for testing, whose C/A code phase was 2430, and the Doppler frequency was 3000 Hz. When the SIR is set to −22 dB, −34 dB, and −38 dB, respectively, the results of the relevant values acquired by the four algorithms for PRN10 are shown in Figures 7–9.

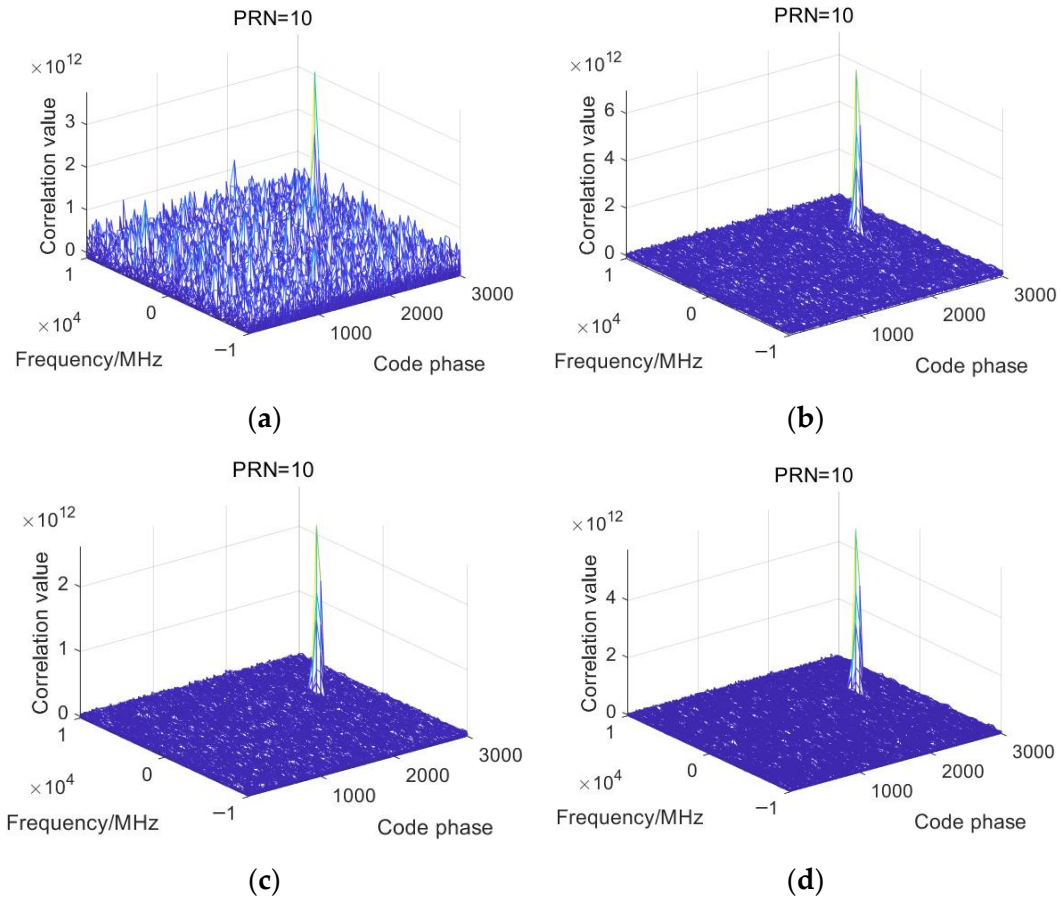

Figure 7. SIR = −22 dB, acquisition effect of the four algorithms: (**a**) coherent integration; (**b**) coherent and non-coherent integration; (**c**) differential coherent integration; and (**d**) improved differential coherent integration.

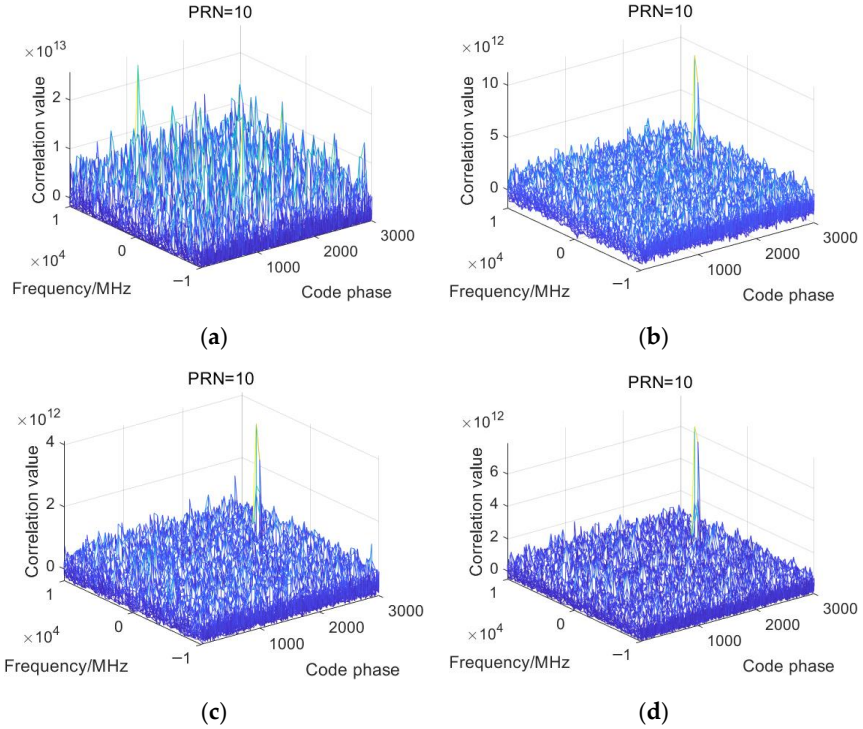

Figure 8. SIR =−34 dB, acquisition effect of the four algorithms: (**a**) coherent integration; (**b**) coherent and non-coherent integration; (**c**) differential coherent integration; and (**d**) improved differential coherent integration.

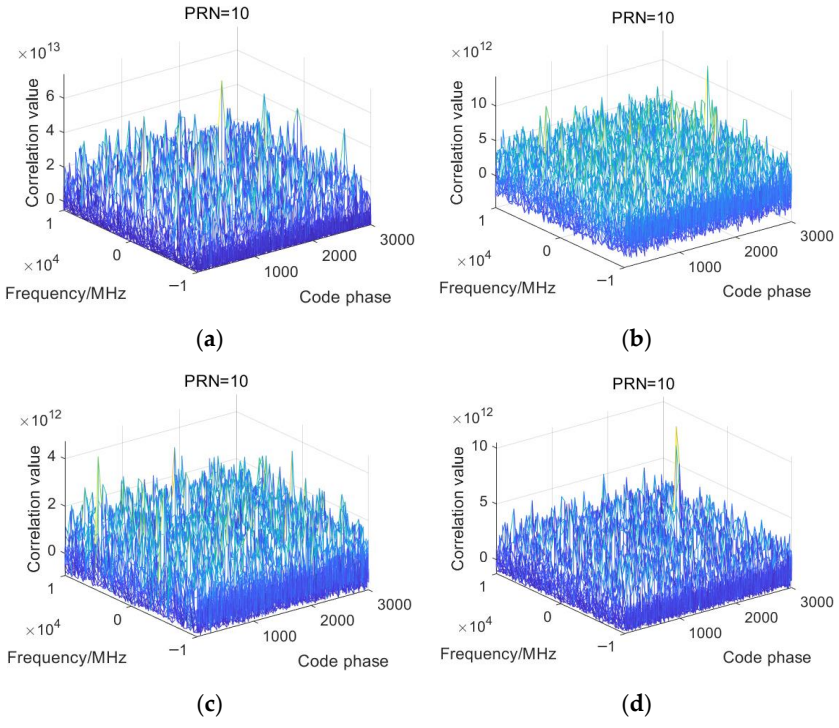

Figure 9. SIR = −38 dB, acquisition effect of the four algorithms: (**a**) coherent integration; (**b**) coherent and non-coherent integration; (**c**) differential coherent integration; and (**d**) improved differential coherent integration.

As can be seen from Figure 7, the correlation peak of the coherent integration is not obvious, while the other algorithms can see obvious peaks with Doppler frequency around

3000 Hz, and the code position is about 2430 code chip. The magnitude of the correlation value of the coherence integral is 10^{13}, and the magnitude of the correlation value of coherent-non-coherent integration, differential coherence integration, and the proposed improved differential coherent integration are all 10^{12}. Because of bit sign transition in coherence integration, the magnitude of the correlation result is lower than that of other methods.

As shown in Figure 8, when the SIR is reduced to −34 dB, the correlation peak of the coherence integral is completely drowned by noise, while an obvious correlation peak can be seen under the other three algorithms.

As can be seen from Figure 9, when the SIR drops to −38 dB, an obvious peak can be detected by the proposed improved differential coherent integration, whereas the correlation peaks of other algorithms were completely drowned by noise. It is proven that the improved algorithm can capture signals in a lower SIR environment.

4.3. Comparison of Acquisition Probability

In order to obtain the acquisition probability under different signal intensity, the Monte Carlo simulation experiment is carried out. Four different algorithms were used to acquire the PRN10 of simulated signals with SIR from −40 to −22 dB. The acquisition probability of the algorithm is obtained every 2000 times under the conditions of the current SIR. The acquisition probability curve is shown in Figure 10.

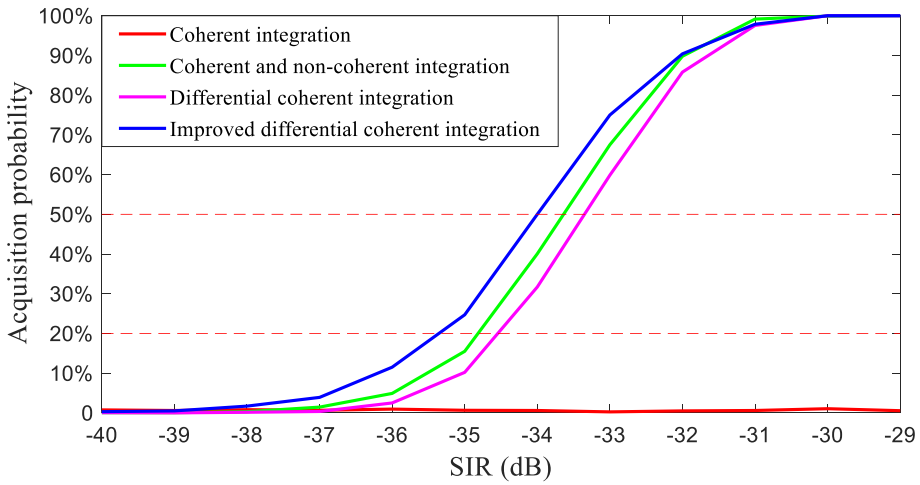

Figure 10. Acquisition probability curve.

When the SIR is greater than −31 dB, except for the coherence integration, the other three acquisition algorithms can complete the signal acquisition. When the SIR is −38~−31 dB, the acquisition probability of improved differential coherent integration is higher than coherent and non-coherent integration and differential coherent integration. Even when the SIR is −34 dB, the acquisition probability of the proposed algorithm can still reach 50%. When the SIR is lower than −36 dB, the acquisition probability of improved differential coherent integration is less than 20%, while the acquisition probability of coherent integration, coherent and non-coherent integration, and differential coherent integration is close to 0. In conclusion, under the condition of low SIR, the acquisition probability of the differential coherent integration combining coherent accumulation and bit sign transition estimation is higher than the other three algorithms, which can acquire signals with low SIR with high acquisition sensitivity.

4.4. Analysis of Acquisition Speed

In terms of computation complexity, assuming that N is the number of sampling points in a coherent integral operation and M is the number of incoherent integral operations, the complex multiplicative quantity required for a correlation operation is $NM\log_2(N)$.

Taking the sampling frequency of 3 MHz simulated in this paper as an example, the complex multiplicative quantity of a single acquisition by the four acquisition algorithms compared in this paper can be obtained, as shown in Table 2. It can be seen that the complex multiplicative quantity of the improved differential coherent integration in this paper is the minimum, with only 21.75% of the highest. Because the coherent accumulation adopted in this algorithm can reduce the number of FFT/IFFT operation points, it is able to achieve a faster acquisition speed.

Table 2. The acquisition speed of the four algorithms.

Acquisition Algorithm	Complex Multiplicative Quantity	Single Acquisition Time
Coherent integration	9.52×10^5	t
Coherent and non-coherent integration	7.53×10^5	0.91 t
Differential coherent integration	1.43×10^6	1.30 t
Improved differential coherent integration	3.11×10^5	0.56 t

Although the absolute computing time depends on different hardware devices and simulation platforms, the time consuming of different algorithms on the same device and platform is also of great significance. Under the circumstance of SIR = −22 dB, the above four methods are tested on the acquisition task of PRN10. Assuming that the single acquisition time of coherent integration is t (t = 0.49375 ms), the acquisition time of other methods is expressed by t with coefficients. Table 2 shows the calculation speed of each algorithm. It can be seen that the improved differential coherent integration is the least, which is less than half of that of the unimproved differential coherence integration.

4.5. Authentic Data Verification

For the authentic signal acquisition experiment, the intermediate frequency data collected in Brazil on 27 February 2014 were played back by the Global Navigation Satellite System signal playback instrument (GNPB-MF) to reproduce the authentic scene when the ionospheric scintillation appeared. Four acquisition algorithms were used to acquire number 19 satellite (PRN19), and continuous 2000 groups of 20 ms data were acquired (total length of data was 40 s). The changes in the amplitude scintillation index (S_4) and carrier-to-noise ratio (C/N_0) in this period are shown in Figure 11.

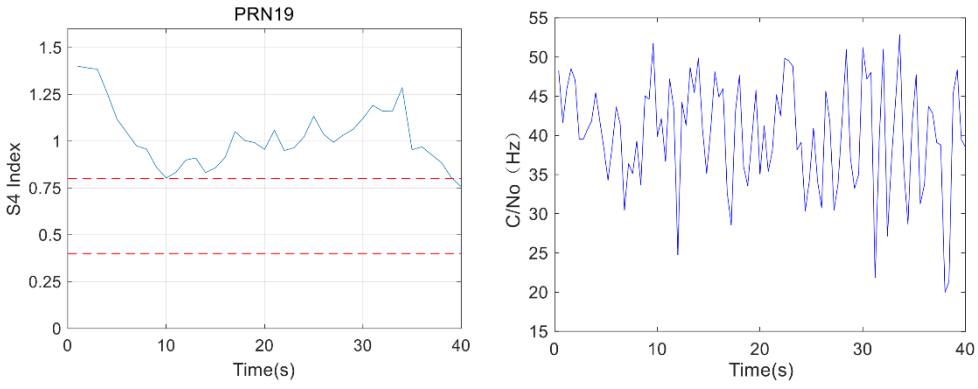

(**a**) (**b**)

Figure 11. Variation diagram of S_4 index and C/N_0 of Brazil data on 27 February 2014; (**a**) S_4, and (**b**) C/N_0.

During this period, PRN19 was interfered by severe ionospheric scintillation, and its C/N_0 fluctuated significantly, with the lowest of only 19.97 dB.

The search step is set at 500 Hz and acquisition threshold at 2.3 to determine the successful acquisition in the test. The Monte Carlo simulation experiment was conducted on the results of the four acquisition methods, and the acquisition probability was generated every 2000 times. The statistics obtained are shown in Table 3. As can be seen from the Table 3 below, the proposed method in this paper has the highest acquisition probability in this authentic severe ionospheric scintillation scenery, reaching 96.1%.

Table 3. Acquisition probability statistics of four algorithms for authentic signals.

Acquisition Algorithm	Acquisition Probability
Coherent integration	61.2%
Coherent and non-coherent integration	95.9%
Differential coherent integration	94.4%
Improved differential coherent integration	96.1%

5. Conclusions and Discussion

In this paper, a weak GPS signal acquisition algorithm based on differential coherent integration combining coherent accumulation and bit sign transition estimation is proposed. The method is based on differential coherent integration and combines coherent accumulation to achieve fast acquisition and reduce noise in signal. Bit sign transition estimation is also used to exclude the data blocks containing bit sign transition, so as to prolong the coherence integration time and realize weak GPS signal acquisition. Comparing the performance of the proposed algorithm with three traditional weak signal acquisition algorithms, the results prove that:

(1) Under the same low SIR condition, the correlation peak of the signal acquired by the proposed method is more obvious, and the acquisition effect is best;
(2) Under the same SIR condition, the proposed method has a higher acquisition probability of 50% when the SIR drops to −34 dB. Under real severe ionospheric scintillation, the acquisition probability of the proposed method is higher than that of traditional methods under the same experimental conditions;
(3) The proposed acquisition algorithm can effectively reduce the computation complexity, which is only 21.75% of the unimproved differential coherence integration, and the acquisition time is less than the unimproved differential coherence integration.

The significance of this research lies in improving the acquisition performance when GNSS signals suffer from serve ionospheric scintillation. It will also be of great guidance in other aspects of interference on GNSS signals. However, the improved acquisition algorithm should be also designed for other types of GNSS signals to avoid bit transition, such as GPS L5 and Beidou signals. In future work, we will focus on designing high-performance tracking and positioning algorithms to impair errors caused by ionospheric scintillation, which will be meaningful for designing an advanced real-time software receiver.

Author Contributions: Conceptualization, M.L. and X.Z.; methodology, G.T. and Y.L.; software, M.L.; validation, Z.L.; formal analysis, Y.L. and M.L.; investigation, Y.L.; resources, X.Z.; data curation, M.L.; writing—original draft preparation, M.L. and Y.L.; writing—review and editing, Z.L.; visualization, M.L.; supervision, G.T. and X.Z.; project administration, X.Z.; funding acquisition, G.T. and X.Z.; All authors have read and agreed to the published version of the manuscript.

Funding: This work was supported by the National Key Research and Development Plan of China (2018YFB0505103), the National Natural Science Foundation of China (61873064) and the Startup Foundation for Introducing Talent of NUIST (2022r073).

Institutional Review Board Statement: Not applicable.

Informed Consent Statement: Not applicable.

Data Availability Statement: Relevant data are available on request from the corresponding author. Please contact to Xuefen Zhu (zhuxuefen@seu.edu.cn).

Conflicts of Interest: The authors declare no conflict of interest.

References

1. Cutugno, M.; Robustelli, U.; Pugliano, G. Low-Cost GNSS Software Receiver Performance Assessment. *Geosciences* **2020**, *10*, 79. [CrossRef]
2. Xie, G. *Principles of GPS and Receiver Design*; Electronics Industry Publishing House: Beijing, China, 2009; pp. 266–384.
3. Chen, X.; He, D.; Pei, L. BDS B1I multipath channel statistical model comparison between static and dynamic scenarios in dense urban canyon environment. *Satell. Navig.* **2020**, *1*. [CrossRef]
4. Breitsch, B.; Morton, Y.J. A Batch Algorithm for GNSS Carrier Phase Cycle Slip Correction. *IEEE Trans. Geosci. Remote Sens.* **2022**, *60*, 1–24. [CrossRef]
5. Geng, W.; Huang, W.; Liu, G.; Liu, S.; Luo, B. Assessing the Kinematic GPS Positioning Performance Under the Effect of Strong Ionospheric Disturbance Over China and Adjacent Areas During the Magnetic Storm. *Radio Sci.* **2022**, *57*, 1–18. [CrossRef]
6. Zhang, Y. Weak Signal Acquisition and Tracking Algorithm Based on the GPS Software Receiver. Master's Thesis, Xi'an University of Science and Technology, Xi'an, China, 2014.
7. Lin, D.; Tsui, J.; Liou, L.; Morton, Y. Sensitivity Limit of a Stand-Alone GPS Receiver and an Acquisition Method. In Proceedings of the International Technical Meeting of the Satellite Division of the Institute of Navigation, Portland, OR, USA, 27 September 2002; pp. 1663–1667.
8. Hussain, A.; Ahmed, A.; Magsi, H.; Soomro, J.B.; Bukhari, S.S.H.; Ro, J.S. Adaptive data length method for GPS signal acquisition in weak to strong fading conditions. *Electronics* **2021**, *10*, 1735. [CrossRef]
9. Elders-Boll, H.; Dettmar, U. Efficient differentially coherent code/Doppler acquisition of weak GPS signals. In Proceedings of the IEEE Eighth International Symposium on Spread Spectrum Techniques & Applications, Sydney, NSW, Australia, 30 August 2004–2 September 2004; pp. 731–735.
10. Huang, H.; Cao, X.; Li, X.; Cao, X. Weak Beidou B1 signal acquisition with bit transitions. *J. Northwest Norm. Univ.* **2019**, *55*, 55–60.
11. Li, S.; Yi, Q.; Chen, Q.; Shi, M. Weak signal acquisition method for GPS software receiver. *J. Comput. Appl.* **2012**, *32*, 816–822. [CrossRef]
12. Jeon, S.; So, H.; Kim, G.; Kee, C.; Kwon, K. Bit transition cancellation signal acquisition method for modernized GPS and Galileo signal. In Proceedings of the International Technical Meeting of the Satellite Division of the Institute of Navigation, Portland, OR, USA, 20–23 September 2011.
13. Borio, D.; O'Driscoll, C.; Lachapelle, G. Coherent, noncoherent, and differentially coherent combining techniques for acquisition of new composite GNSS signals. *IEEE Trans. Aerosp. Electron. Syst.* **2009**, *45*, 1227–1240. [CrossRef]
14. Savas, C.; Falco, G.; Dovis, F. A Comparative Performance Analysis of GPS L1 C/A, L5 Acquisition and Tracking Stages under Polar and Equatorial Scintillations. *IEEE Trans. Aerosp. Electron. Syst.* **2021**, *57*, 227–244. [CrossRef]
15. Kai, B.; Dennis, M.; Nicolaj, B.; Peter, R.; S∅ren, H. . *A Software-Defined GPS and Galileo Receiver*; Springer: Berlin, Germany, 2006; pp. 75–86.
16. Li, X.; Guo, W. Efficient Differential Coherent Accumulation Algorithm for Weak GPS Signal Bit Synchronization. *IEEE Commun. Lett.* **2013**, *17*, 936–939.
17. Zeng, D.; Ou, S.; Li, J.; Sun, J.; Li, H. Analysis and Comparison of Non-coherent and Differential Acquisition Integration Strategies. In Proceedings of the China Satellite Navigation Conference (CSNC) 2015 Proceedings, Xi'an, China, 13–15 May 2015; pp. 163–176.
18. Gu, J.; Yan, G.; Yang, J. High Sensitivity Fast Acquisition Algorithm for GPS Software Receiver Signal. *Fire Control Command. Control* **2019**, *44*, 67–71.
19. Cheng, Y.; Chang, Q.; Li, X. Avoiding Bit Transition Acquisition Algorithm for Weak GPS Signal. *Navig. Position. Timing* **2017**, *4*, 94–99.
20. Zhang, Y. Research on Beidou Weak Signal Acquisition and Tracking Algorithm. Master's Thesis, Fuzhou University, Fuzhou, China, 2018.